Available online at www.sciencedirect.com
ScienceDirect
Journal of Nuclear Materials 374 (2008) 61–68
journal of nuclear materials
www.elsevier.com/locate/jnucmat

High-resolution imaging of complex crack chemistry in reactor steels by NanoSIMS

S. Lozano-Perez [a,*], M.R. Kilburn [a,b], T. Yamada [c], T. Terachi [c], C.A. English [d], C.R.M. Grovenor [a]

[a] Department of Materials, University of Oxford, Parks Road, OX1 3PH Oxford, UK
[b] Centre for Microscopy and Microanalysis, University of Western Australia, 35 Stirling Hwy, Crawley 6009 WA, Australia
[c] Institute of Nuclear Safety Systems Inc, 64 Sata, Mikata-gun, Fukui 919-1205, Japan
[d] Nexia Solutions, Harwell Business Centre, Didcot, Oxon OX11 0RA, UK

Received 25 April 2007; accepted 13 July 2007

Abstract

High-resolution analysis using a Cameca NanoSIMS 50 has been used to map the oxide chemistry in intergranular cracks in stainless steels. The technique has proven ideal for this type of sample, as it is able to discern between the different oxide layers and clarify the role of minor segregants such as boron and sulphur. Results are compared with analysis of the same sample by scanning auger microscopy and its interpretation discussed. The short time required to prepare and examine multiple regions present the NanoSIMS as an optimum tool for corrosion characterization.

PACS: 82.80.Ms; 62.20.Mk; 68.37.Xy; 62.20.Mk

1. Introduction

Environmentally assisted cracking is one of the least understood and most important degradation phenomena in predicting the safe lifetime of structural steels. The complex interaction of environment, microstructure and mechanical loading requires analysis by a wide range of different techniques in order to obtain a complete picture of the critical processes and mechanisms. In particular, the mechanisms controlling stress corrosion cracking (SCC) and irradiation-assisted stress corrosion cracking (IASCC) of austenitic steels and Ni based alloys employed in nuclear reactor components need to be properly understood if reliable predictions of lifetime are to be achieved [1–4].

Considerable effort has been placed on characterising the detailed morphology and internal structure of cracks in SCC specimens originating from laboratory tests and in samples extracted from operating plants [5–8]. The primary objective of these studies is to gain an improved understanding of the critical phenomena controlling SCC, and have revealed, for example, characteristic narrow oxide-filled cracks in the case of nickel alloys, details of the oxide microstructure, evidence of porosity and details of interaction of cracks with dislocations, defects and precipitates in the surrounding metallic matrix.

It is clear that the characterization of cracks in samples subjected to SCC should provide information at high spatial resolution (≈1–10 nm) on:

1. Oxide composition, including levels of minor constituents such as B, P and S. These trace impurities are known to have a strong influence on intergranular fracture [9–13]. In particular it is important to obtain composition profiles across the crack flanks and crack tip and in the metal matrix immediately ahead of the crack tip.

* Corresponding author.
E-mail address: Sergio.lozano-perez@materials.ox.ac.uk (S. Lozano-Perez).

0022-3115/$ - see front matter © 2007 Elsevier B.V. All rights reserved.
doi:10.1016/j.jnucmat.2007.07.009

2. Oxide structure both at the crack flanks and at the crack tip. Information on oxide porosity, orientation relationships with the surrounding metal matrix, and how the oxide grows with respect to the original grain boundary is also of value. Of importance is also the interaction of any oxide with crystallographic features such as dislocations, deformation bands or twins.
3. Information on the metal matrix containing the crack(s), for example grain orientation, grain boundary parameters, dislocation density in the material adjacent to the crack tip and flank.

A schematic representation of a crack is shown in Fig. 1. to illustrate the features described above. It is also important to examine a sufficient number of individual cracks to identify typical behaviour. This has been a particular problem in the past in studies relying heavily on TEM analysis.

Characterisation of cracks successfully addressing these requirements has come predominantly from studies in modern transmission electron microscopes (TEMs) with the latest analytical capabilities [5,14]. Such studies necessarily involve complex and time- consuming specimen preparation to obtain electron transparent samples from the crack flank and crack tip. In addition, it is only possible to examine a very restricted region of cracks within the sample. Techniques where a larger volume and more statistically significant number of cracks may be examined have been employed; for example traditional surface characterization methods including scanning electron microscopy (SEM), scanning auger microscopy (SAM) and secondary ion mass spectroscopy (SIMS) [15–18]. To date none has been able to demonstrate the required high spatial resolution and high elemental sensitivity necessary to provide chemical information to compare with that available from the TEM.

In this paper we will describe, for the first time, the benefits of using a Cameca NanoSIMS for characterizing stress corrosion cracks, and demonstrate that it has a major role to play, particularly for improved insight into the oxide composition and the influence of crystallographic features on oxide formation.

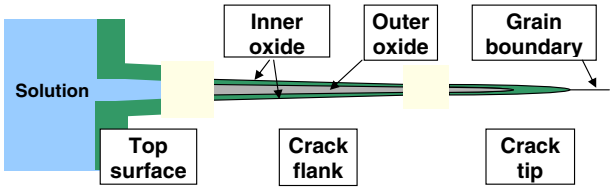

Fig. 1. Schematic representation of a stress corrosion crack and its representative features.

2. Material

The materials employed in this study are a type 304 stainless steel (SUS304) and two 304-like alloys that have lower Cr levels but with the levels of other alloying elements chosen to match the original SUS304 composition (12Cr and 15Cr). Type 304 stainless steel (SUS304) is widely used in Pressurised Water Reactors (PWRs) and Boiling Water Reactors (BWRs). The compositions of the alloys used are shown in Table 1. All alloys were solution treated (SUS304 at 1060 °C for 100 min and 12Cr and 15Cr alloys at 1100 °C for 100 min) and then water-quenched. The specimens were cold-rolled to a reduction of 20% prior to testing. They will be referred as 20% cold work (20% cw).

The SCC test was performed using a 1/2T CT specimen, under constant load and a simulated PWR primary water chemistry (500 ppm B + 2 ppm Li, + 30 cm^3-STP/kg-H_2O DH_2) at 320 °C. The SCC test lasted 666 h and produced intergranular cracks over 100 μm in length. Some samples were fatigued after testing in order to complete the fracture.

3. Methodology

Samples with a suitable geometry for NanoSIMS analysis (9 mm diameter and 1 mm thick disks) were extracted from the bulk samples using a spark eroder machine. Once mounted in suitable holders, they were polished with 1200 SiC paper, 3 μm diamond paste and finished with silica suspension (with 0.04 μm average grain size). This was the only sample preparation required for effective analysis of crack chemistry.

In this work, both primary and secondary cracks were examined. A primary or dominant crack is defined as a crack which is growing throughout the test as a result of the applied stress and the corrosive environment. A secondary crack might have been dominant at some point during propagation but it was overrun by another crack, being left behind and exposed to the environment for a longer period of time, mostly under a lower stress than that experienced by the primary crack. These secondary cracks are normally located near triple points and they are normally found filled by magnetite.

Table 1
Chemical content of examined alloys (wt%)

Alloy	Fe	C	Si	Mn	P	S	Ni	Cr	Mo
20% cw SUS304	Bal.	0.04	0.31	1.6	0.003	0.001	9.2	18.3	<0.01
20% cw 15Cr	Bal.	0.06	0.5	1.5	0.002	0.001	10	15.0	<0.01
20% cw 12Cr	Bal.	0.06	0.5	1.6	0.002	0.001	9.6	12.0	<0.01

Analyses were performed using the Cameca NanoSIMS 50 in the Department of Materials, University of Oxford. A Cs^+ primary beam, focused to less than 50 nm, was used to sputter negative secondary ions from the sample surface. Secondary ions were mapped on five detectors simultaneously. The ion species analysed were $^{12}C^-$, $^{16}O^-$, $^{11}B^{16}O_2^-$, $^{32}S^-$, $^{58}Ni^-$, $^{52}Cr^{16}O^-$, and $^{56}Fe^{16}O^-$, on masses 12, 16, 32, 43, 58, 68 and 72, respectively. The mass spectrometer was calibrated using pure metallic Ni, Cr and Fe standards, and tuned to high mass resolution to eliminate any isobaric interferences.

The areas containing the features of interest were cleaned prior to examination by scanning a defocused primary beam over the surface for up to 1 h, depending on the initial surface condition. Images were acquired by scanning a 0.5 pA primary beam over areas ranging from 5 to 35 μm square. Image resolutions of 512×512 or 256×256 pixels, with count times of up to 40 ms per pixel, were obtained. Ion induced secondary electron images were acquired concurrently. The octopoles controlling the symmetry of the probe were tuned before each acquisition to ensure a stigmatism-free image. In eight days of operation, with morning and afternoon sessions, more than 100 regions were analyzed.

In order to assess the value of these observations in the NanoSIMS, a comparison has been made to TEM examination of specimens obtained from the same samples, and also with TEM samples of equivalent samples examined in previous studies. In addition, a comparison has been made with observations in a scanning auger microscope of identical regions to those examined in the NanoSIMS. For convenience these comparisons will be presented in the results section.

4. Results

For each of the alloys shown in Table 1, several cracks and their associated features were analyzed using the NanoSIMS. Both primary and secondary cracks have been analysed. A cross-sectional view of the 20% cw SUS304 sample after testing, cutting and polishing can be seen in Fig. 2. The fatigue pre-crack is at the bottom of the image, oriented vertically. The strain direction was applied perpendicular to this crack, and it is indicated by the arrow. Once the crack region is located using the in-situ CCD camera in the NanoSIMS, the positions of the relevant features (crack tips, triple points, etc.) are stored and a series of analysis performed. Up to 15 regions were analyzed per day, enabling all the dominant cracks and most of the secondary cracks visible on the surface of each sample to be characterized.

4.1. Information from composition mapping

A typical example of the information obtainable in the NanoSIMS is shown in Fig. 3. In this figure, major element distributions in the oxide formed on the flanks of a secondary crack in the 20% cw 15Cr alloy are shown. The oxides found always consist of an inner Cr-rich layer and an outer

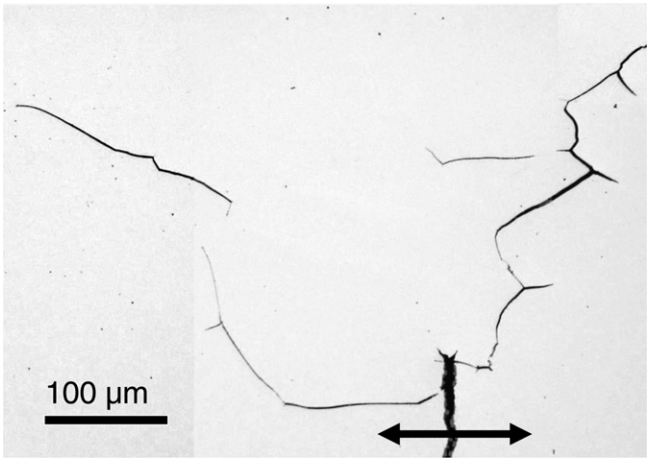

Fig. 2. Optical micrograph showing a bifurcated stress corrosion crack in a 20% cw SUS304 sample after the test. The wider crack at the bottom of the image is the fatigue pre-crack lying perpendicular to the strain direction (indicated by the arrow).

Fe-rich oxide which tends to fill the crack as it opens (see Fig. 1 for definition of inner and outer). This observation is in agreement with previous work, showing a double oxide layer in similarly tested 304 alloys [14,19]. In Fig. 4, results from a STEM observations of a similar sample are shown. The dark-field (DF) STEM image shows a portion of a secondary crack, which was found to be filled by oxides. Interpretation of the structure is easier with the aid of EDX elemental maps, which are also shown in Fig. 4. It can be seen that the inner oxide layer is Cr-rich (depleted in Fe but not in Cr), and the outer is formed by Fe-rich oxide crystals. From electron diffraction data it has been established that the inner layer is Cr-rich spinel and that the outer oxide is magnetite. The Ni levels in the oxides have also been shown to be lower than the original metallic bulk level. The linear features intersecting the crack are discussed below.

In order to check the quality of the results obtained by the NanoSIMS, the same area shown in Fig. 3 was analyzed with a scanning auger microscope (see Fig. 5). The operating conditions were as follows; beam energy of 10 kV, beam current of 10 nA and beam size of ≈27 nm. Maps were acquired with 256×256 pixels, 0.7 ms dwell time and 15 frames. In Fig. 5. it can be seen that all the elemental maps look very similar to those acquired with the NanoSIMS (Fig. 3), however, a more detailed analysis of the data reveals that the NanoSIMS provides a better signal-to-noise ratio (SNR) in all elements analyzed, as shown in the "discussion" section. In addition, the ability in the NanoSIMS to analyze molecular ions like $^{56}Fe^{16}O^-$ and $^{52}Cr^{16}O^-$ makes it much easier to identify the oxidized nature of the fine Cr-rich region in the crack flanks.

These linear features extending from the crack flank in Figs. 3 and 5 were used to make a detailed comparison of the compositional information obtained in the NanoSIMS and with SAM. The O signal across the linear feature (arrowed in Fig. 3) gives a signal-to-noise ratio (SNR) of

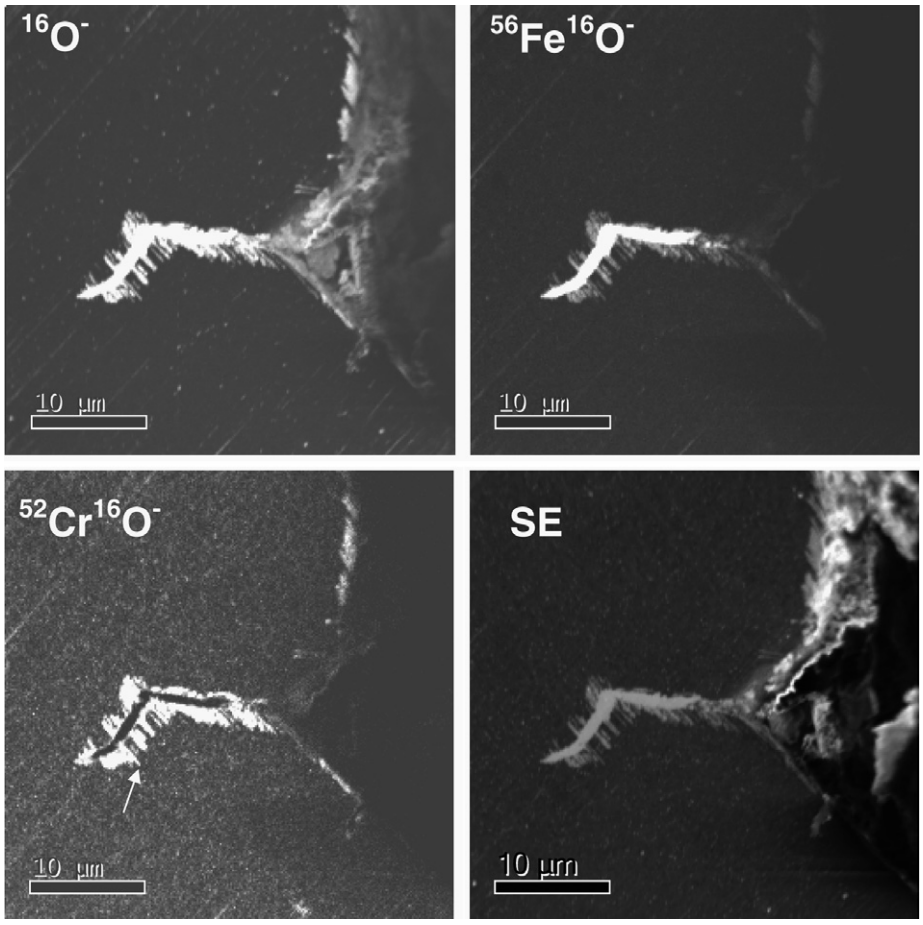

Fig. 3. NanoSIMS maps and SE imagefrom a secondary crack in the 20% cw 15Cr sample.

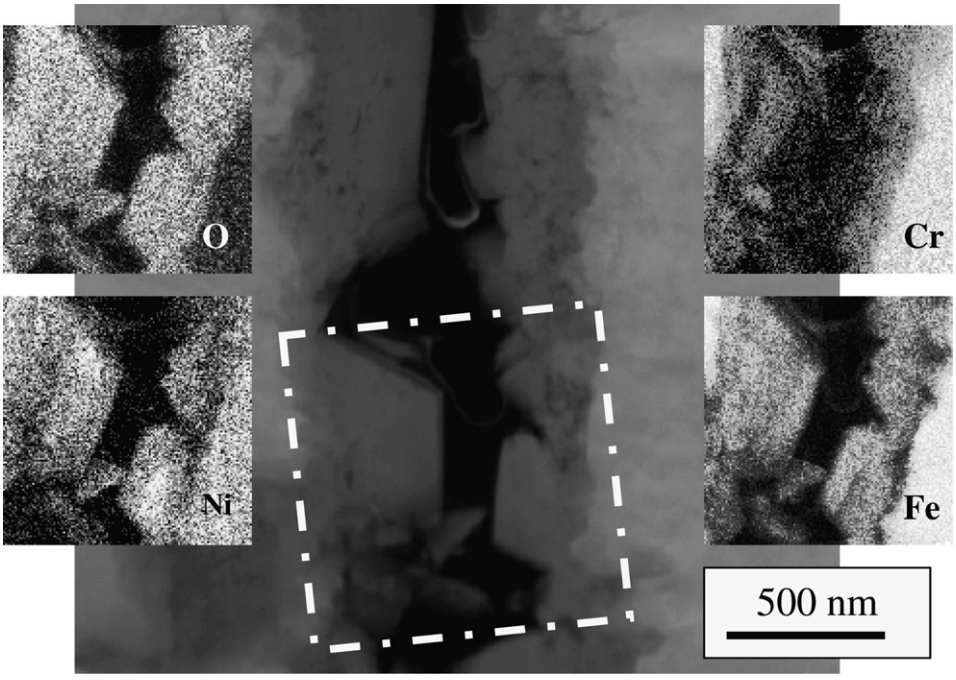

Fig. 4. DF STEM image showing a secondary crack flank in a SUS304 sample (without cw). On the sides, STEM EDX elemental maps are shown for O, Cr, Ni and Fe.

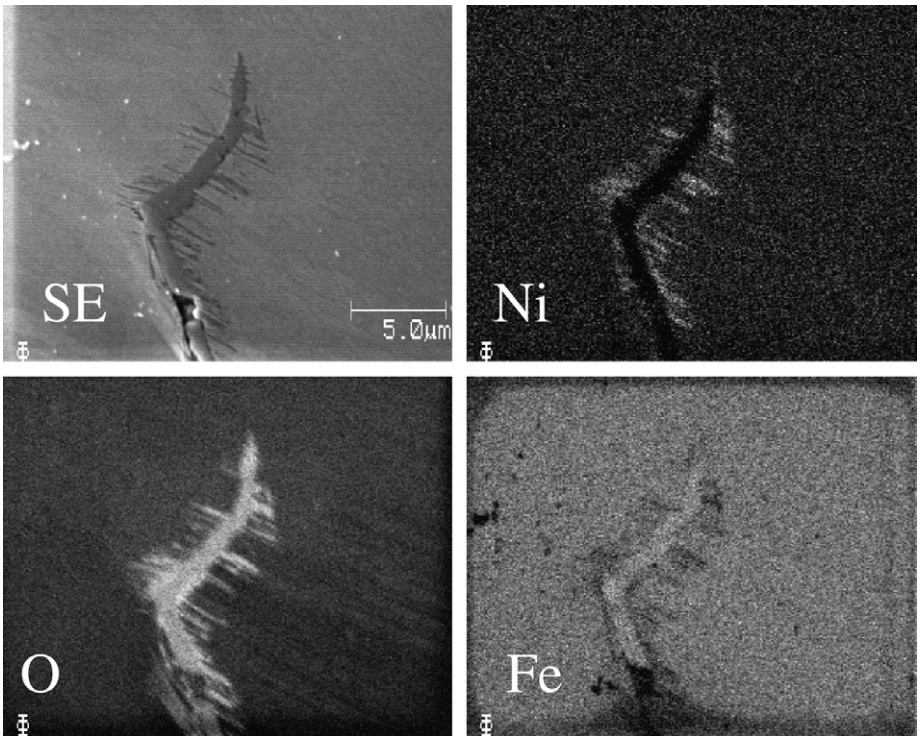

Fig. 5. SAM maps from same region as in Fig. 3.

5 using the NanoSIMS and 1.8 in the Auger equivalent map (Fig. 5). The standard deviation of the data in the surrounding matrix is relatively similar. For the O map, σ is 20% of the mean value in the Auger map and 18% in the NanoSIMS. The spatial resolution achieved by the two techniques looks comparable at around 50 nm.

The NanoSIMS can also be a powerful tool for the study of trace element distributions around cracks because of the very high sensitivity of SIMS analysis for many impurities in steel samples. A NanoSIMS line profile across the Cr-rich oxide layer of the flank of the fatigue pre-crack in the 20% cw SUS304 alloy is presented in Fig. 6. to illustrate the detection of minor constituents of the oxide. Line profiles were measured directly from the ion images, which were acquired using 10 ms/pixel and a current of 7.9 nA. All profiles have been normalized in order to account for the different yields. Boron is enriched at the original sample interface, while S seems to diffuse deeper. No traces of B could be found by EDX or EELS analysis in the TEM samples extracted from the crack tip region of a secondary crack in the 20% cw 15Cr alloy. In addition, in regions of the crack flank, where B was observed in the NanoSIMS (with a SNR of ≈25), no B was detected in the scanning auger microscope.

4.2. Oxide interaction with the crystallographic features in the matrix

The NanoSIMS cannot provide data (other than composition) that allows the structure of the oxides to be iden-

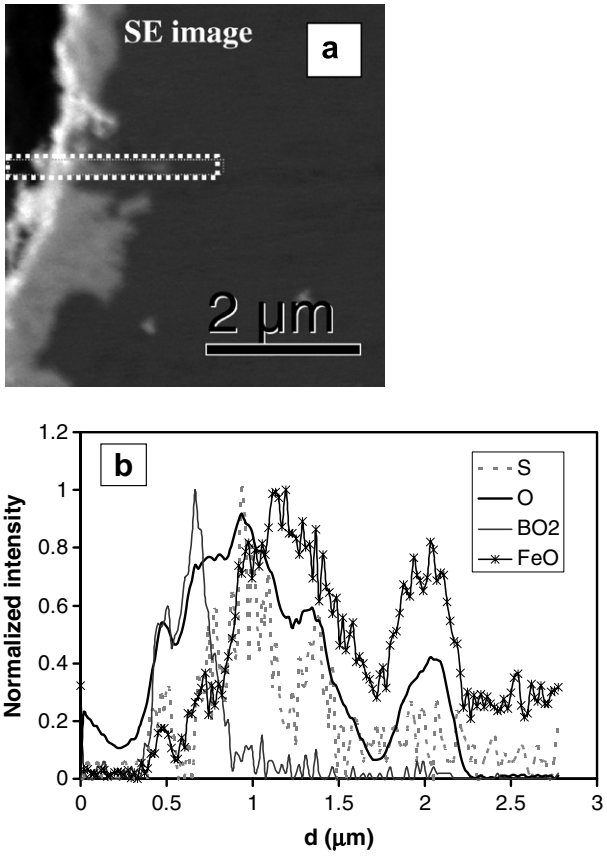

Fig. 6. Detail of surface oxidation in the 20% cw SUS304 sample. (a) SE image showing the position of line profile (b) NanoSIMS line profile results (normalized to unity).

tified, although this can be provided by conventional TEM techniques. However, it has been found in this study that the ability to characterise extensive regions of crack flanks and a number of crack tips in several samples enables information to be obtained in a systematic manner on the influence of pre-existing crystallographic features in the metal matrix on subsequent oxide formation.

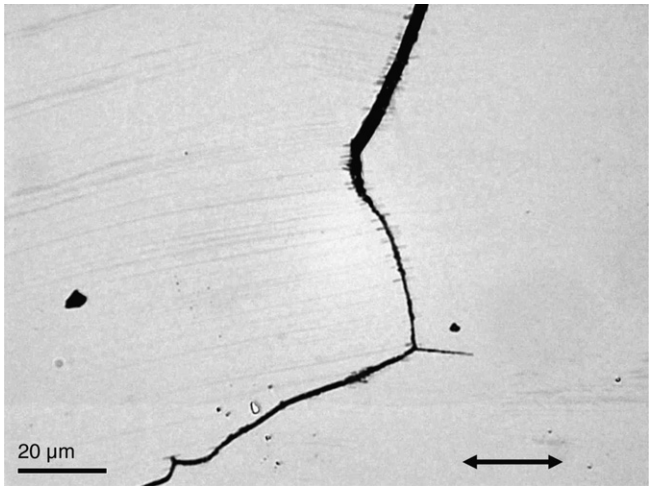

Fig. 7. Optical micrograph showing a portion of a SC crack in the 20% cw 15Cr alloy. Deformation bands along slip directions can be seen as a result of the slight etching caused by the silica polishing. The arrow represents the strain direction.

In Fig. 7 deformation along slip bands in the grain interiors can be seen as a result of the slight etching caused by the silica polishing in the 20% cw 15 Cr alloy. NanoSIMS images of similar regions in the 20% cw 12Cr alloy are shown in Fig. 8. It is clear that the enhanced contrast next to the crack flank is actually due to formation of a Cr-rich oxide along these deformation bands. It can also be seen that there the oxide contains Fe but that, as expected, Ni levels are reduced (since it is rejected by the formation of Cr-rich oxide). It is also obvious that each grain oxidises differently.

Observations from the NanoSIMS have also enabled preliminary interpretations on how the oxide at a crack tip forms in relation to the grain boundary chemistry. In Fig. 9, a dominant crack tip has been analyzed in the 20% cw SUS304 alloy and some line profiles have been measured from the crack tip region along the continuing grain boundary. Both $^{56}Fe^{16}O^-$ and $^{11}B^{16}O_2^-$ maps are shown to aid the interpretation. The $^{11}B^{16}O_2^-$ map is very useful as it shows B segregation to the grain boundary, thus enabling its location in the matrix to be determined at the same time as studying the crack and grain boundary chem-

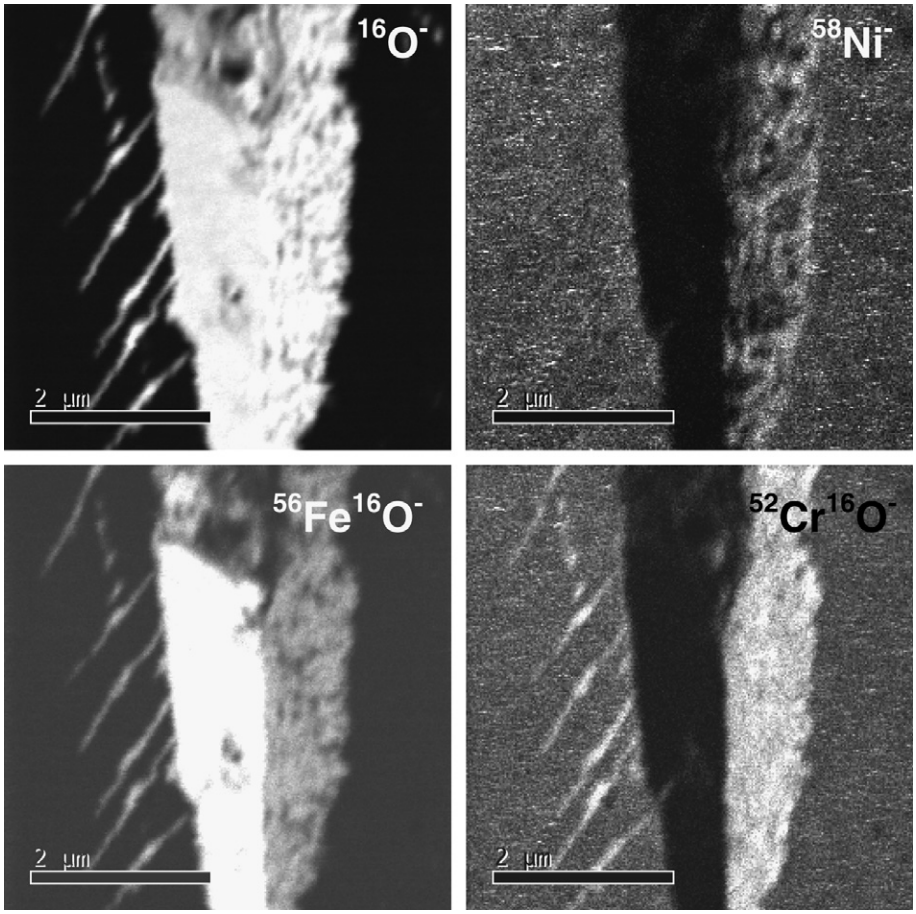

Fig. 8. NanoSIMS maps showing the dominant crack in the 20% cw 12Cr sample.

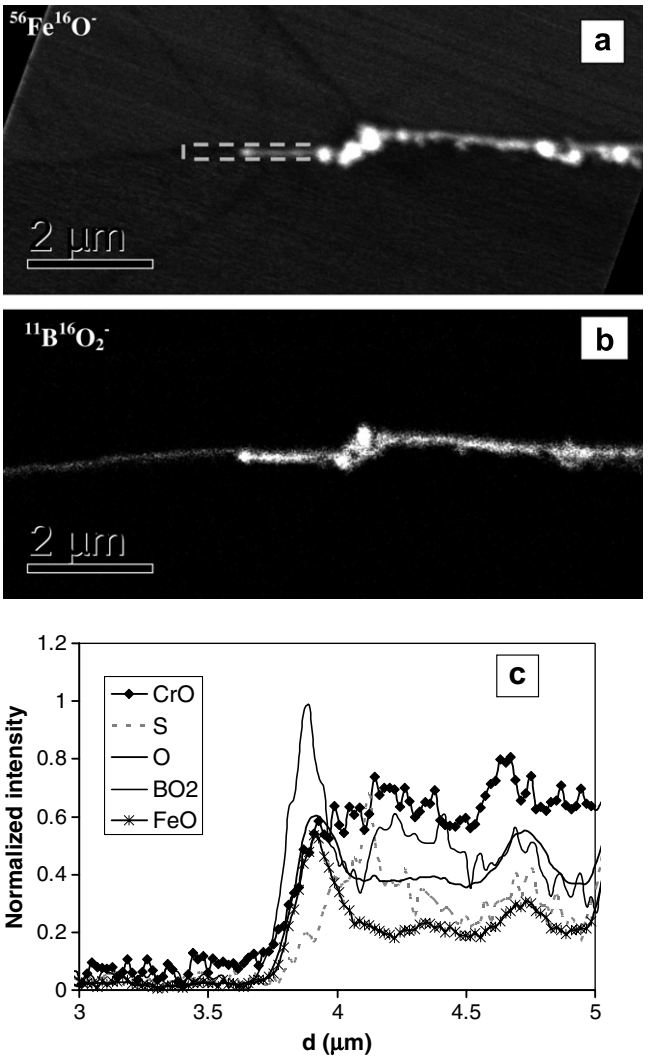

Fig. 9. Dominant crack tip region in the 20% cw SUS304 sample (a) NanoSIMS $^{56}Fe^{16}O^-$ map showing the position of line profile (b) NanoSIMS $^{11}B^{16}O_2^-$ map from same region and (c) NanoSIMS line profiles (normalized to unity).

istry. It can also be seen that oxidation occurs preferentially on the bottom grain, possibly due to its more favourable crystallographic orientation.

5. Discussion and conclusions

The high lateral resolution of the NanoSIMS together with the high chemical sensitivity to certain elements means that it can be an important new tool in establishing a multiscale approach to the study of stress corrosion cracks in steels. The benefits of applying the NanoSIMS are:

- Ease of sample preparation. It has to be emphasised that the elaborate preparation techniques necessary for TEM or atom probe analysis are not required for NanoSIMS, making the analysis quick and easy to perform.
- A lateral spatial resolution of less than 50 nm for the major elements found in the oxides associated with cracks.
- Ability to detect both major elements (Cr, Fe and Ni) and also minor elements such as S, P and B. It is to be noted that S and B segregation in these samples could not be detected using TEM or SAM.

The major disadvantage is that the necessary calibrations for the yield of the elements of interest in a steel matrix have not been performed in the NanoSIMS, preventing the acquisition of truly quantitative data at this stage. All the data shown in this work is thus qualitative. Several random grain boundaries were analyzed in the bulk (a few mm far from the cracked region) in order to confirm the observed B segregation to grain boundaries. A similar B enrichment was observed. Due to the high yield of B, NanoSIMS is able to detect concentrations of the order of ppm. As mentioned before, no B was observed at boundaries with any of the other techniques, so its enrichment is expected to be well below 1 at.%.

Critically, in a typical experimental campaign on the NanoSIMS a significant number of cracks can be examined. This has two benefits; firstly the oxide structures in different cracks can be compared and 'typical behaviour' established, and secondly, regions for subsequent examination in the TEM or atom probe can be identified. This way, these higher resolution techniques, which involve time-consuming specimen preparation, can be focussed on the critical regions.

A detailed analysis of the crack flank and crack tip region has provided very important information. Firstly, the results agree with previously reported observations of a dual oxide layer consisting of an inner Cr-rich oxide layer and an outer Fe-rich oxide layer (see Fig. 4) [14,15,19]. Second, it has been possible to observe oxide penetrating along crystallographic deformation bands into the adjacent grain. This observation has not been found in the literature and more detailed analysis of the relation between oxide formation along deformation bands and surrounding grains microstructure is being performed. These observations might have important implications on the mechanisms of crack propagation and are currently being investigated into more detail.

In conclusion, the high lateral and mass resolution together with the high sensitivity of the NanoSIMS provide a unique tool for the extensive investigation of stress corrosion cracks in stainless steels. Information with fine detail complementing that obtained by TEM, but with better chemical sensitivity, was easily obtained on polished bulk samples. No special sample preparation was necessary. It has been shown that the NanoSIMS can provide information on the oxide composition with a resolution good enough to separate the different oxide layers. It also provides detailed compositional profiles across/along features of interest and very valuable information on the distribution of minor segregants (S, B).

Acknowledgements

Dr Lozano-Perez is grateful to INSS (Japan) for fully supporting his work and providing the samples used in this

work. Professors Brian Eyre and George Smith are acknowledged for their encouraging comments and useful discussion. The NanoSIMS was purchased under UK EPSRC grant GR/M61023.

References

[1] P.L. Andresen, P.W. Emigh, L. Young, in: INSS (Ed.), International Symposium on the Mechanisms of Materials Degradation and Non-destructive Evaluation in LWR, 2004, p. 3.
[2] P.L. Andresen, F.P. Ford, in: Proceedings of the Third International Symposium on Environmental Degradation of Materials in Nuclear Power Systems – Water Reactors, 1987, p. 789.
[3] P.L. Andresen, F.P. Ford, Mater. Sci. Eng. A 103 (1988) 167.
[4] K. Arioka, T. Yamada, T. Terachi, R.W. Staehle, Corrosion 62 (2006) 74.
[5] S.M. Bruemmer, L.E. Thomas, Surf. Interface Anal. 31 (2001) 571.
[6] L.E. Thomas, S.M. Bruemmer, Corrosion 56 (2000) 572.
[7] S. Lozano-Perez, J.M. Titchmarsh, M.L. Jenkins, in: J. Engelbretch, T. Sewell, M. Witcomb, R. Cross, P. Richards (Eds.), Proceedings of the ICEM15, Microscopy Society of Southern Africa, Onderstepoort, South Africa, 2002, p. 787, September.
[8] G.S. Was, J.K. Sung, T.M. Angeliu, Metall. Trans. 23A (1992) 3343.
[9] G.C. Allen, P.E.J. Flewitt, P. McIntyre, C. Preece, R.K. Wild, C.M. Younes, Mater. Sci. Forum (1996) 453.
[10] D.G. Briceno, M.I. Castano, S. Garcia, Proceedings of the International Conference, Chemistry in Water Reactors: Operating Experience and New Developments 2 (1994) 719.
[11] J.M. Titchmarsh, S. Dumbill, J. Microsc. 188 (1997) 224.
[12] I.A. Vatter, J.M. Titchmarsh, Surf. Interface Anal. 25 (1997) 760.
[13] A. Cerezo, T.J. Godfrey, C.R.M. Grovenor, G.D.W. Smith, J. Phys.: Conden. Matter 1 (1989) 99.
[14] S. Lozano-Perez, J.M. Titchmarsh, M.L. Jenkins, in: S. McVitie, D. McComb (Eds.), Proceedings of the EMAG2003, Inst. of Phys. Publishing, 2003, p. 233, 3–5 September.
[15] T. Terachi, K. Fujii, K. Arioka, J. Nucl. Sci. Technol. 42 (2005) 225.
[16] G. Santarini, Corrosion 45 (1989) 369.
[17] F. Delabrouille, L. Legras, F. Vaillant, P. Scott, B. Viguier, E. Andrieu, in: T.R. Allen, P.J. King, L. Nelson (Eds.), Proceedings of the 12th International Conference on Environmental Degradation of Materials in Nuclear Power Systems-Water Reactors, TMS (The Minerals, Metals & Materials Society), USA, 2006, p. 903.
[18] P. Scott, M. Foucault, B. Brugier, J. Hickling, A. McIlree, in: T.R. Allen, P.J. King, L. Nelson (Eds.), Proceedings of the 12th International Conference on Environmental Degradation of Materials in Nuclear Power Systems-Water Reactors, TMS (The Minerals, Metals & Materials Society), USA, 2006, p. 497.
[19] S. Lozano-Perez., PhD thesis, University of Oxford, 2002.